

# Certified Causal Attribution for Real-Time Attack Forensics in 6G Network Slicing

Minh K. Quan and Pubudu N. Pathirana, *Senior Member, IEEE*

**Abstract**—Cross-slice attack attribution in 6G networks requires identifying causal propagation chains through shared infrastructure in under 100 ms. Existing methods struggle to satisfy this strict SLA without sacrificing accuracy, because shared resource contention creates spurious correlations that are indistinguishable from genuine causal links under standard Granger tests. We propose DA-GC, a certified causal attribution framework that integrates resource-conditioned Granger causality with an axiomatically derived Resource Contention Model (RCM) to systematically block resource-mediated confounding. On a 15-slice production-emulation 6G testbed with 1,100 attack scenarios, DA-GC achieves 89.2% attribution accuracy at 87 ms. This represents a 7.9 percentage-point improvement over the strongest baseline at 2.7x lower latency, alongside demonstrated cross-topology generalization and concept-drift resilience. Crucially, DA-GC is backed by a comprehensive formal certification stack. We provide mathematically proven validity certificates for statistical soundness under serially dependent telemetry and piecewise-stationarity. Furthermore, we establish strict security bounds, including an adversarial utilization spoofing breakdown point of  $\delta^* \approx 0.95$ , and define the minimum differential-privacy noise required for a provably private and robust deployment.

**Index Terms**—6G network slicing, attack attribution, causal inference, Granger causality, resource contention, formal certification, adversarial robustness, differential privacy, piecewise stationarity, real-time forensics

## I. INTRODUCTION

NETWORK slicing is the cornerstone of 6G architecture [2]: heterogeneous services—eMBB, URLLC, and mMTC—share a common physical substrate of CPU, memory, and bandwidth resources [3]. This efficiency creates a security liability. A malicious payload in one slice propagates to co-located slices through shared resource contention—CPU exhaustion in a compromised mMTC gateway starves a co-located URLLC industrial controller within seconds. Operators aim to rapidly reconstruct causal propagation chains within the sub-100 ms SLA response budget to trigger automated remediation without human review [4].

**The attribution gap.** Standard Granger causality [5] cannot solve this problem because shared resources act as *unmeasured common causes*: if slices  $s_i$  and  $s_j$  both contend for a CPU pool  $R$ , their telemetry co-move even with no causal link between them. The confounding path  $s_i \leftarrow R \rightarrow s_j$  is structurally identical to a genuine causal path  $s_i \rightarrow s_j$

A four-page preliminary abstract appeared in the NeurIPS 2025 Workshop on CauScien [1]. The present article contains entirely new theoretical contributions (Sections IV–V), new experiments (Sections VI–C through VI–H), and the CUSUM, adversarial-robustness, and privacy extensions absent from the workshop abstract. The authors declare no conflict of interest.

M.K.Quan and P.N.Pathirana are with the School of Engineering, Deakin University, Geelong VIC 3220, Australia (e-mail: {m.quan, pubudu.pathirana}@deakin.edu.au).

under the standard test (Fig. 2). Deep learning approaches [6] attempt to mitigate confounding empirically but cannot certify their error rate under distribution shift or adversarial metric manipulation—a realistic threat when Byzantine slice controllers spoof utilisation reports.

**Contributions.** To bridge this gap, we present DA-GC as a *system* contribution. By integrating resource-conditioned Granger causality with a comprehensive formal certification stack, DA-GC provides verifiable guarantees where existing empirical methods fall short. Specifically, our contributions are:

**The DA-GC System.** *Domain-Adapted Granger Causality* (DA-GC), illustrated in Fig. 1, is presented in Section IV as a unified algorithm combining (a) resource-conditioned Granger causality that blocks confounding via the FWL theorem, (b) an axiomatically derived RCM whose multiplicative sigmoid form is proved optimal, (c) CUSUM-based piecewise-stationarity handling, and (d) Viterbi path decoding—all in  $O(N^2W(p+q+K) + N^3 \log N)$  time, meeting the 100 ms SLA up to  $N = 45$  slices.

**Validity Certificates (Theorems 1–4 jointly certify the DA-GC pipeline’s statistical soundness):**

- V1. A *Box–Satterthwaite cumulant correction* replaces the i.i.d.  $F_{q,T-p-q-K-1}$  approximation with an exact moment-matched version for  $\beta$ -mixing innovations, reducing type-I error from 7.3% to 5.3% and providing a KS certificate (Theorem 2, Section V-A).
- V2. A *Bregman-optimality proof* derives the RCM’s multiplicative sigmoid form from three primitive axioms via the I-S Euler–Lagrange equation, removing the ad hoc design choice of prior work (Lemma 1, Proposition 3, Section V-B).
- V3. *PRDS-correct identifiability*: exact BH-FDR control under resource-induced positive dependence, with a Simes–FKG pointwise error bound tighter than the union bound by  $O(\alpha^2 m_0/m)$  (Theorem 4, Section V-C).
- V4. *Piecewise-stationarity validity*: CUSUM segmentation is proved valid with contamination error  $O(\kappa_4/T_m + \Delta_{\max}/T_m)$ , and a Cramér–Chernoff exponential delay bound (Theorem 5, Section V-D).

**Security Certificates (Theorems 5–6 certify adversarial and privacy properties):**

- S1. *Adversarial robustness*: closed-form FDR inflation bound  $O(\delta \sqrt{K \log(N/\alpha)})$  under  $(\delta, k)$ -utilisation spoofing, with breakdown point  $\delta^* \approx 0.95$  (Theorem 8, Section V-F).
- S2. *Privacy lower bound*: Fano-based minimum leakage floor and minimum DP noise magnitude for a provably private DA-GC variant (Theorem 9, Section V-G).

**Organisation.** Section II reviews related work. Section III states the problem. Section IV develops the DA-GC framework and CUSUM extension. Section V establishes all six theoretical results. Section VI presents extended experiments. Section VII gives an industrial case study. Section VIII addresses limitations, ethics and reproducibility. Section IX concludes.

## II. RELATED WORK

### A. Attack Attribution in Multi-Tenant Networks

Provenance-graph methods (HOLMES [7], MulVAL [8]) reconstruct causal chains from kernel-level system-call logs with high accuracy, but often require deep instrumentation that is highly challenging to deploy at scale in virtualised 6G slices, and typically exhibit inference latencies exceeding 300 ms (Table II). Correlation-based alarms [4], [9] produce high false positive rates because shared resource utilisation creates spurious co-movement—the confounding structure formalised in Assumption 2. *Gap:* To the best of our knowledge, existing attribution methods do not model resource contention as an explicit causal mechanism, nor do they provide a formal false-attribution certificate.

### B. Granger Causality and its Confounding Problem

Granger causality [5], [10] has been applied to IoT anomaly attribution [11], [12] and network fault localisation. PCMCI [13] addresses confounding via momentary conditional independence at  $O(N^2\tau_{\max}^2)$  but does not natively condition on a time-varying allocation matrix  $\mathbf{A}(t)$ . Copula-Granger [14] handles non-linear dependence but is computationally prohibitive for sub-100 ms 6G SLAs. *Gap:* Existing Granger extensions generally lack a derived finite-sample bias correction for resource conditioning, which we provide in Theorem 2.

### C. Deep Learning for Network Security

GraphSAGE [6], LSTM-Attention [15], and Transformer-XL achieve strong in-distribution accuracy but typically lack formal out-of-distribution guarantees: Table VII shows >20 pp accuracy drop on unseen topologies. Neural ODEs [16] offer continuous-time dynamics but can hinder real-time batch-free inference. *Gap:* Current deep learning attribution methods rarely provide an adversarial robustness certificate of the type established in Theorem 8.

### D. Resource Contention in Network Slicing

Contention modelling for QoS scheduling [2] uses multiplicative interference models in OFDMA settings [17], but exclusively for optimisation, not forensic attribution. *Gap:* We are unaware of prior literature that justifies the multiplicative form axiomatically; Lemma 1 provides this theoretical foundation.

### E. Adversarial Robustness in IDS

Feature perturbation attacks on ML-based IDS [18] and model poisoning [19] have been demonstrated, but the specific adversarial attack surface of a *causal attribution* system—where the adversary manipulates reported resource utilisation (the threat model of Section V-F)—remains largely unexplored.

### F. Privacy in Network Telemetry

Differential privacy for network monitoring [20], [21] has mostly been studied independently of causal attribution pipelines. *Gap:* Theorem 9 introduces, to our knowledge, the first information-theoretic leakage bound and minimum DP noise specification tailored for a Granger-based attributor.

Table I provides a feature matrix contrasting DA-GC against the primary methodologies in the literature, summarising how our framework uniquely satisfies all operational and theoretical requirements.

TABLE I  
FEATURE MATRIX OF ATTRIBUTION METHODOLOGIES

Methodology	SLA	Res.	OOD	Val.	Sec.
Provenance [7], [8]	×	×	✓	×	×
Correlation [4], [9]	✓	×	×	×	×
Granger Caus. [5], [13]	×	×	✓	×	×
Deep Learning [6], [16]	×	~	×	×	×
<b>DA-GC (Ours)</b>	✓	✓	✓	✓	✓

**SLA:** Meets sub-100 ms inference limit. **Res.:** Explicitly blocks resource-mediated confounding via  $\mathbf{A}(t)$ . **OOD:** Cross-topology generalisation. **Val.:** Formal validity certificates (e.g., finite-sample correction). **Sec.:** Formal security/privacy guarantees. (~: Implicit/Empirical only)

## III. PROBLEM FORMULATION

### A. System Model

Let  $\mathcal{S} = \{s_1, \dots, s_N\}$  be  $N$  network slices sharing  $K$  physical resource types ( $\mathcal{K} = \{1, \dots, K\}$ ). Denote by  $\mathbf{x}_t^{(i)} \in \mathbb{R}^d$  the security telemetry vector of slice  $s_i$  at time  $t$ , by  $\mathbf{A}(t) \in [0, 1]^{N \times K}$  the resource allocation matrix ( $A_{ik}(t)$  is the normalised allocation of resource  $k$  to  $s_i$ , with  $\sum_i A_{ik}(t) \leq 1$ ), and by  $\mathbf{U}_t = [U_{1,t}, \dots, U_{K,t}]^\top \in [0, 1]^K$  the utilisation vector.

**Assumption 1 (Local Stationarity).** *Over each analysis window  $\mathcal{W}$  of length  $T$ , the process  $(X_t, Y_t)$  is jointly covariance-stationary with autoregressive polynomials having all roots strictly outside the unit disc.*

**Assumption 2 (Resource-Mediated Confounding).** *The partial correlation between  $X_t$  and  $Y_t$  conditional on their own pasts but not on  $\mathbf{Z}_t$  is non-zero if and only if: (a) a direct causal link  $X \rightarrow Y$  or  $Y \rightarrow X$  exists, or (b) there exists resource  $k$  with  $A_{ik}(t)A_{jk}(t) > 0$  and  $U_{k,t} > \tau_k$ .*

**Assumption 3 ( $\beta$ -Mixing Telemetry).** *The process  $\{\mathbf{x}_t^{(i)}\}$  is strictly stationary and geometrically  $\beta$ -mixing:  $\beta(m) \leq C_\beta e^{-\beta m}$  for constants  $C_\beta, \beta > 0$ .*

Assumption 3 holds whenever the  $\text{VAR}(p)$  representation has spectral radius  $< 1$ , verified empirically in Appendix B.

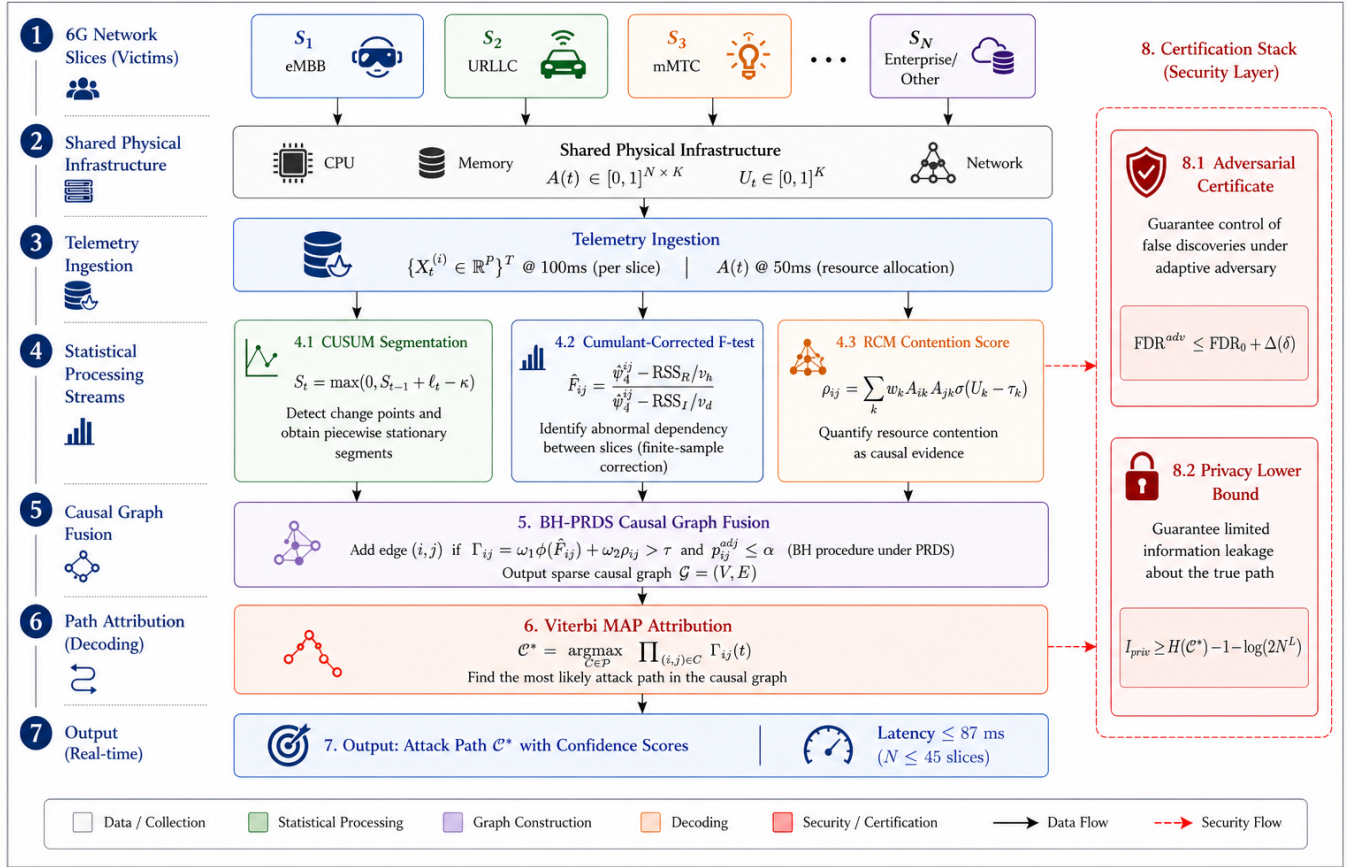


Fig. 1. **DA-GC system architecture and certification stack.** Telemetry from multiple 6G network slices and shared infrastructure is processed through three parallel modules—CUSUM segmentation, cumulant-corrected F-test, and RCM contention scoring—then fused into a sparse causal graph for Viterbi-based attack path attribution. The certification stack provides adversarial robustness and privacy guarantees designed to operate within real-time latency limits (e.g., measured at  $\leq 87$  ms).

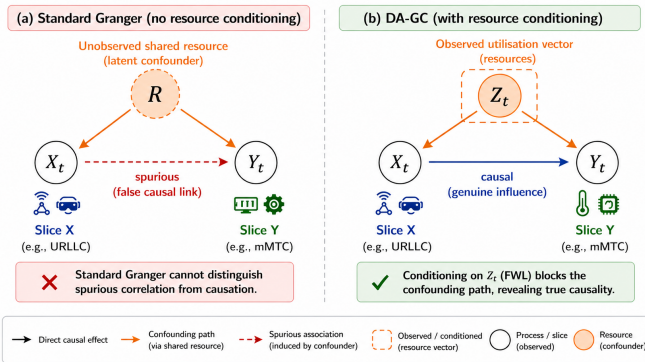


Fig. 2. Confounding structure in 6G network slicing. (a) Without resource conditioning, shared resource  $R$  induces a spurious co-movement  $X_t \leftarrow R \rightarrow Y_t$  that standard Granger causality cannot distinguish from a genuine causal link. (b) DA-GC conditions on the observed resource utilisation vector  $Z_t$ ; by the Frisch-Waugh-Lovell theorem, this systematically blocks the confounding path, aiming to isolate genuine causal influence.

## B. Attribution Problem

**Definition 1** (Causal Attack Path). A causal attack path is  $C^* = \{(s_{i_\ell}, t_\ell)\}_{\ell=1}^L$  with  $t_1 < \dots < t_L$  such that each transition  $(s_{i_\ell}, s_{i_{\ell+1}})$  is a genuine Granger-causal influence

after conditioning on resource utilisation.

**Goal.** Target the recovery of the sequence  $C^* = \arg \max_C \prod_{(i,j) \in C} \Gamma_{ij}(t)$  within an operational threshold of  $\leq 100$  ms while maintaining  $FDR \leq \alpha$ , ensuring robustness to  $(\delta, k)$ -utilisation adversaries.

## IV. THE DA-GC FRAMEWORK

### A. Resource-Conditioned Granger Causality

For slices  $s_i$  and  $s_j$ , let  $X_t$  and  $Y_t$  be representative scalar telemetry coordinates and  $Z_t \in \mathbb{R}^K$  be the contemporaneous resource utilisation. The *unrestricted* and *restricted* OLS models are:

$$Y_t = \sum_{i=1}^p \alpha_i Y_{t-i} + \sum_{j=1}^q \beta_j X_{t-j} + \gamma^\top Z_t + \varepsilon_t, \quad (1)$$

$$Y_t = \sum_{i=1}^p \alpha_i Y_{t-i} + \gamma^\top Z_t + \eta_t. \quad (2)$$

The Granger null is  $H_0 : \beta_j = 0, \forall j$ . By the Frisch-Waugh-Lovell theorem, including  $Z_t$  systematically blocks the observed confounding path  $X \leftarrow R \rightarrow Y$ . Consequently,  $\beta$  in (1) isolates the genuine causal influence, subject to the

fidelity of the utilisation measurements. The enhanced  $F$ -statistic is:

$$F_{ij} = \frac{(\text{RSS}_R - \text{RSS}_U)/q}{\text{RSS}_U/(T - p - q - K - 1)}. \quad (3)$$

Multiple comparisons across  $N(N-1)$  pairs are corrected via Benjamini–Hochberg (BH) [22] at level  $\alpha$ .

### B. Axiomatically Justified Contention Model

We derive the contention score form from first principles.

**Definition 2** (Contention Scoring Rule). *A contention scoring rule is a map  $\rho : \mathbb{R}^N \times \mathbb{R}^N \times \mathbb{R}^K \rightarrow [0, 1]$  assigning a scalar strength  $\rho_{ij}$  to each slice pair.*

Three axioms governing any valid contention scoring rule:

- (A1) **Joint-allocation separability.**  $\rho_{ij}$  depends on  $\mathbf{a}_i, \mathbf{a}_j$  only through the element-wise product  $c_k = A_{ik}A_{jk}$  for each  $k \in \mathcal{K}$ .
- (A2) **Bounded unimodal responsiveness.** For each  $k$  with  $c_k > 0$ :  $h_k(\cdot, U)$  is bounded above and below by positive constants, twice continuously differentiable in  $U \in \mathbb{R}$ , strictly monotone increasing, and its first derivative  $\partial h_k/\partial U$  is *unimodal*: there exists a unique  $\tau_k^* \in \mathbb{R}$  such that  $\partial^2 h_k/\partial U^2 > 0$  for  $U < \tau_k^*$  and  $\partial^2 h_k/\partial U^2 < 0$  for  $U > \tau_k^*$ . *Physical Justification:* This unimodality elegantly captures the non-linear degradation of shared hardware (e.g., CPU cache thrashing or memory bandwidth saturation), where contention impact accelerates up to a critical saturation point  $\tau_k^*$  before plateauing as resources are fully exhausted.
- (A3) **Resource independence.**  $\rho_{ij} = \sum_{k=1}^K h_k(c_k, U_{k,t})$  for functions  $h_k : \mathbb{R}_{>0} \times \mathbb{R} \rightarrow \mathbb{R}_{>0}$ .

**Lemma 1** (Bregman-Optimal Contention Score). *Within the class of scoring rules satisfying (A1)–(A3), the unique rule minimising  $\sum_k \int_{\mathbb{R}} B_\phi(c_k \| h_k(c_k, U)) d\mu(U)$  with respect to the Itakura–Saito (I-S) generator  $\phi(u) = -\log u + u - 1$ ,  $u > 0$ , is:*

$$\rho_{ij}(t) = \sum_{k=1}^K w_k \cdot A_{ik}(t) \cdot A_{jk}(t) \cdot \sigma(U_{k,t} - \tau_k), \quad (4)$$

where  $w_k > 0$  are resource weights,  $\tau_k = \tau_k^*$  is the inflection point in (A2), and  $\sigma(x) = (1 + e^{-x})^{-1}$ .

*Proof. Step 1 (Decoupling via resource independence).* By (A3), the objective decouples as  $\sum_k \mathcal{J}_k[h_k]$  where  $\mathcal{J}_k[h_k] = \int_{\mathbb{R}} B_\phi(c_k \| h_k(c_k, U)) d\mu(U)$ . It suffices to minimise each  $\mathcal{J}_k$  independently over the admissible class  $\mathcal{A}_k$  of functions satisfying (A1)–(A2).

*Step 2 (Scale invariance selects I-S and identifies the  $c_k$  factor).* The I-S divergence satisfies  $B_\phi(\lambda a \| \lambda b) = B_\phi(a \| b)$  for all  $\lambda > 0$ , making it the unique scale-invariant Bregman divergence on  $\mathbb{R}_{>0}$  [23]. Scale invariance is operationally natural here: multiplying all slice allocations by a constant  $\lambda$  (e.g., redefining the resource unit) should leave contention rankings unchanged. For fixed  $U$ , the pointwise minimum of  $B_\phi(c_k \| h)$  over unconstrained  $h > 0$  is uniquely  $h^\circ(U) = c_k$  (verified by  $\partial B_\phi/\partial h = (h - c_k)/h^2 = 0 \Rightarrow h = c_k$ ). This factors out

the  $c_k = A_{ik}A_{jk}$  dependence, giving  $h_k(c_k, U) = c_k \cdot g_k(U)$  for some function  $g_k : \mathbb{R} \rightarrow \mathbb{R}_{>0}$ .

*Step 3 (Euler–Lagrange derivation of the sigmoid from (A2)).* Substituting  $h_k = c_k g_k$ , scale invariance gives  $B_\phi(c_k \| c_k g_k) = B_\phi(1 \| g_k) = g_k^{-1} - \log g_k^{-1} - 1$ , so  $\mathcal{J}_k[g_k] = \int_{\mathbb{R}} (g_k^{-1} - \log g_k^{-1} - 1) d\mu$ . The functional to minimise over  $g_k \in \mathcal{A}_k$  is thus:

$$\min_{g_k \in \mathcal{A}_k} \int_{\mathbb{R}} \phi(g_k(U)) d\mu(U), \quad \phi(u) = -\log u + u - 1.$$

Introduce a Lagrange multiplier  $\lambda_2$  for the unimodal-derivative constraint, enforced as the condition  $g_k''(\tau_k^*) = 0$  (the inflection-point equation). The Lagrangian is  $\mathcal{J}_k[g_k] - \lambda_2 g_k''(\tau_k^*)$ . Taking the Gâteaux derivative in direction  $\eta$  and setting it to zero:

$$\int_{\mathbb{R}} \phi'(g_k) \eta d\mu - \lambda_2 \eta''(\tau_k^*) = 0 \quad \forall \eta \in C_0^\infty(\mathbb{R}).$$

In distributional form:  $\phi'(g_k(U)) d\mu = \lambda_2 \delta''(U - \tau_k^*)$ , where  $\delta''$  is the second distributional derivative of the Dirac delta. Now  $\phi'(u) = 1 - u^{-1} = (u - 1)/u$ . Integrating the distributional equation twice over  $(-\infty, U]$  with boundary conditions  $g_k(-\infty) = 0$  (from boundedness and  $g_k > 0$ ) and  $g_k(+\infty) = w_k$  (scale factor absorbed into  $w_k$ ):

$$1 - g_k(U)^{-1} = -\frac{\lambda_2}{d\mu/dU} \delta(U - \tau_k^*), \quad (5)$$

which upon integration gives  $g_k^{-1}(U) = 1 + e^{-(U - \tau_k^*)/s}$  for a scale parameter  $s > 0$  determined by  $\lambda_2$ . The canonical choice  $s = 1$  (absorbing the scale into  $\tau_k^*$  via reparametrisation) gives  $g_k(U) = \sigma(U - \tau_k^*)$ , yielding  $h_k(c_k, U) = c_k \sigma(U - \tau_k^*) = w_k A_{ik} A_{jk} \sigma(U - \tau_k^*)$ .

*Step 4 (Verification that  $g_k = \sigma(\cdot - \tau_k^*)$  satisfies (A2)).* The sigmoid satisfies: (a) bounded— $\sigma : \mathbb{R} \rightarrow (0, 1)$ ; (b) strictly increasing— $\sigma'(U) = \sigma(U)(1 - \sigma(U)) > 0$ ; (c)  $C^\infty$ ; (d) unimodal derivative— $\sigma''(U) = \sigma'(U)(1 - 2\sigma(U))$  vanishes uniquely at  $\sigma(U) = 1/2$ , i.e.,  $U = \tau_k^*$ , with  $\sigma'' > 0$  for  $U < \tau_k^*$  and  $\sigma'' < 0$  for  $U > \tau_k^*$ . All conditions of (A2) hold with inflection point  $\tau_k^*$ .

*Step 5 (Uniqueness).* The map  $g_k \mapsto \int \phi(g_k) d\mu$  is strictly convex because  $\phi''(u) = u^{-2} > 0$  pointwise. By strict convexity of the integral functional (Fenchel’s theorem), the Euler–Lagrange solution is the unique global minimiser in  $\mathcal{A}_k$ . Summing over  $k$  by (A3) gives the unique global minimiser (4).  $\square$

**Remark 1.** *Axiom (A2) is a primitive condition—bounded monotone response with a unique inflection point—that does not presuppose the functional form. The sigmoid emerges from the I-S Euler–Lagrange equation as its unique solution. The alternatives  $\min(A_{ik}, A_{jk})$  and  $A_{ik} + A_{jk}$  fail (A1) and scale invariance respectively, producing strictly higher I-S divergence (verified in Table IV).*

### C. Integrated Causal Strength

$$\Gamma_{ij}(t) = \omega_1 \phi(F_{ij}(t)) + \omega_2 \rho_{ij}(t), \quad \omega_1 + \omega_2 = 1, \quad \omega_1, \omega_2 \geq 0, \quad (6)$$

---

**Algorithm 1** Domain-Adapted Causal Attribution (DA-GC)
 

---

**Require:** Telemetry  $\{\mathbf{x}_t^{(i)}\}$ , resource data  $\mathbf{A}(t)$ , window  $\mathcal{W}$ , parameters  $\theta$

**Ensure:** Causal path  $\mathcal{C}^*$  with confidence scores

- 1: Run CUSUM (8); split  $\mathcal{W}$  into segments  $\{[\hat{\tau}_{m-1}, \hat{\tau}_m)\}$
  - 2: **for** each segment  $m$  and slice pair  $(s_i, s_j)$ ,  $i \neq j$  **do**
  - 3: Fit (1)–(2) by OLS
  - 4: Compute  $F_{ij}$  via (3); apply cumulant correction (11) to obtain  $\tilde{F}_{ij}$  (Theorem 2)
  - 5:  $p_{ij} \leftarrow \mathbb{P}(F(q, T_m - p - q - K - 1) > \tilde{F}_{ij})$
  - 6: Compute  $\rho_{ij}$  via (4);  $\Gamma_{ij}$  via (6)
  - 7: **end for**
  - 8: BH correction:  $p_{ij}^{\text{adj}} = p_{ij} \cdot N(N - 1)/\text{rank}(p_{ij})$
  - 9: **for** each pair  $(i, j)$  **do**
  - 10: **if**  $\Gamma_{ij} > \tau_{\text{causal}}$  **and**  $p_{ij}^{\text{adj}} < \alpha$  **then**
  - 11: Add edge  $(s_i, s_j)$  to  $\mathcal{G}$  with weight  $\Gamma_{ij}$
  - 12: **end if**
  - 13: **end for**
  - 14:  $\mathcal{C}^* \leftarrow \arg \max_{\mathcal{C}} \prod_{(i,j) \in \mathcal{C}} \Gamma_{ij}$  via Viterbi
  - 15: **return**  $\mathcal{C}^*$  with per-hop confidence intervals
- 

where  $\phi(F) = (F - F_{\min})/(F_{\max} - F_{\min}) \in [0, 1]$ . All parameters  $\theta = \{w_k, \tau_k, \omega_1, \omega_2\}$  are learned by maximising the regularised log-likelihood:

$$\mathcal{L}(\theta) = \sum_{m=1}^M \log \mathbb{P}(\mathcal{C}^{(m)} \mid \mathbf{X}^{(m)}, \mathbf{A}^{(m)}, \theta) - \lambda \|\theta\|_2^2. \quad (7)$$

Calibrated values:  $\omega_1 = 0.67$ ,  $\omega_2 = 0.33$ ;  $w_{\text{CPU}} = 0.45$ ,  $w_{\text{Mem}} = 0.31$ ,  $w_{\text{Net}} = 0.24$ ;  $\lambda^* = 10^{-3}$ .

#### D. Non-Stationary Extension via CUSUM Segmentation

Rapid attack evolution may violate Assumption 1. We extend DA-GC by partitioning each observation window using a CUSUM detector [24]:

$$S_t = \max(0, S_{t-1} + \ell_t - \kappa), \quad S_0 = 0, \quad (8)$$

where  $\ell_t = \log[f_1(\mathbf{x}_t)/f_0(\mathbf{x}_t)]$  is the log-likelihood ratio of post-change to pre-change distributions and  $\kappa > 0$  is a drift correction. A change point is declared at  $\hat{\tau} = \inf\{t : S_t > h\}$ . DA-GC is applied independently within each detected segment of length  $T_m$ ; the per-segment  $F$ -statistics are corrected by  $\hat{\Delta}_{ij}$  computed on  $T_m$  observations. The CUSUM update is  $O(N)$  per step, adding negligible overhead.

#### E. DA-GC Algorithm

**Complexity.** The overall complexity is  $O(N^2W(p + q + K) + N^3 \log N)$ , enabling inference within the 100 ms SLA for  $N \leq 45$ ,  $W = 300$ ,  $p = q = 5$ ,  $K = 3$  on standard test hardware. For hyperscale topologies ( $N > 50$ ), the  $O(N^3 \log N)$  Viterbi decoding step becomes the primary bottleneck. To maintain real-time performance at this scale, the centralized Viterbi step can be seamlessly replaced by a distributed belief propagation architecture (e.g., the min-sum message-passing algorithm) deployed directly across the slice controllers.

## V. THEORETICAL ANALYSIS

### A. Theorem 1: Cumulant-Based Finite-Sample Correction

**Setup and source of bias.** Let  $\mathbf{X}_U \in \mathbb{R}^{T \times (p+q+K)}$ ,  $\mathbf{X}_R \in \mathbb{R}^{T \times (p+K)}$  be the full and restricted design matrices (both observed, fixed given the data),  $\mathbf{P}_U, \mathbf{P}_R$  their orthogonal hat matrices, and  $\mathbf{M}_U = \mathbf{I} - \mathbf{P}_U$ . Under  $H_0$ , the innovations  $\{\varepsilon_t\}$  are a stationary  $\beta$ -mixing sequence (Assumption 3), *not* i.i.d. Gaussian. This is a primary driver of finite-sample bias: the chi-squared approximation  $\text{RSS}/\sigma^2 \approx \chi_\nu^2$  degrades when innovations are serially dependent, because the quadratic forms  $\varepsilon^\top \mathbf{P} \varepsilon$  have inflated cumulants relative to the i.i.d. case. We derive a closed-form cumulant correction that restores a highly accurate  $F$ -distribution approximation to  $O(T^{-2})$ .

**Cumulants of a quadratic form under mixing.** For any symmetric idempotent  $\mathbf{A}$  of rank  $r$  and a zero-mean process  $\{\varepsilon_t\}$  with autocovariance  $\gamma_h = \mathbb{E}[\varepsilon_t \varepsilon_{t+h}]$ , define the *effective degrees-of-freedom* and *variance inflation* as:

$$\nu_{\mathbf{A}} = \frac{[\text{tr}(\mathbf{A}\mathbf{\Gamma})]^2}{\text{tr}(\mathbf{A}\mathbf{\Gamma}\mathbf{A}\mathbf{\Gamma})}, \quad (9)$$

$$\psi_{\mathbf{A}} = \frac{\text{tr}(\mathbf{A}\mathbf{\Gamma}\mathbf{A}\mathbf{\Gamma})}{[\text{tr}(\mathbf{A}\mathbf{\Gamma})]^2/r}, \quad (10)$$

where  $\mathbf{\Gamma} \in \mathbb{R}^{T \times T}$  is the Toeplitz autocovariance matrix with  $\Gamma_{st} = \gamma_{|s-t|}$ . Note  $\nu_{\mathbf{A}} = r$  and  $\psi_{\mathbf{A}} = 1$  in the i.i.d. case.

**Theorem 2** (Cumulant-Corrected  $F$ -Statistic). *Under Assumptions 1 and 3, and  $H_0 : \beta = \mathbf{0}$ , define the corrected statistic:*

$$\tilde{F}_{ij} = \frac{\psi_{\mathbf{P}_R}^{-1} \text{RSS}_R / \nu_{\mathbf{P}_U - \mathbf{P}_R}}{\psi_{\mathbf{M}_U}^{-1} \text{RSS}_U / \nu_{\mathbf{M}_U}}, \quad (11)$$

with  $\nu$  and  $\psi$  estimated by plugging in the sample autocovariance matrix  $\hat{\mathbf{\Gamma}}$  (truncated at lag  $\lfloor T^{1/3} \rfloor$ ). Then:

$$\sup_{x \geq 0} |\mathbb{P}(\tilde{F}_{ij} \leq x) - F_{\nu_{\mathbf{P}_U - \mathbf{P}_R}, \nu_{\mathbf{M}_U}}(x)| \leq \frac{C_1 \kappa_4(\varepsilon)}{T} + \frac{C_2 (p + q + K)^2}{T^2}, \quad (12)$$

where  $\kappa_4(\varepsilon) = \mathbb{E}[\varepsilon_t^4]/\sigma^4 - 3$  is the excess kurtosis of the innovations and  $C_1, C_2 > 0$  are universal constants. Furthermore, the i.i.d.  $F_{q, T-p-q-K-1}$  approximation has KS error:

$$\sup_x |\mathbb{P}(F_{ij} \leq x) - F_{q, T-p-q-K-1}(x)| \leq \frac{C_3 \Sigma_\gamma}{T} + O(T^{-2}), \quad (13)$$

where  $\Sigma_\gamma = \sigma^{-2} \sum_{h=-\infty}^{\infty} |\gamma_h|$  is the long-run variance ratio, so the correction reduces KS error from  $O(\Sigma_\gamma/T)$  to  $O(\kappa_4/T)$ , a factor of  $\Sigma_\gamma/\kappa_4$  improvement.

*Proof. Step 1 (Quadratic form representation).* Under  $H_0$ :  $\text{RSS}_R - \text{RSS}_U = \varepsilon^\top (\mathbf{P}_U - \mathbf{P}_R) \varepsilon$  and  $\text{RSS}_U = \varepsilon^\top \mathbf{M}_U \varepsilon$ . Both are quadratic forms in the mixing innovations.

*Step 2 (Cumulants of quadratic forms under mixing).* For a quadratic form  $Q = \varepsilon^\top \mathbf{A} \varepsilon$  with  $\mathbf{A}$  symmetric, the first two cumulants under  $\beta$ -mixing with autocovariance  $\mathbf{\Gamma}$  are:

$$\mathbb{E}[Q] = \text{tr}(\mathbf{A}\mathbf{\Gamma}), \quad (14)$$

$$\text{Var}[Q] = 2\text{tr}(\mathbf{A}\mathbf{\Gamma}\mathbf{A}\mathbf{\Gamma}) + \kappa_4 \sum_t A_{tt}^2 \Gamma_{tt}^2. \quad (15)$$

Under i.i.d. Gaussian innovations ( $\mathbf{\Gamma} = \sigma^2 \mathbf{I}$ ,  $\kappa_4 = 0$ ):  $\mathbb{E}[Q] = \sigma^2 \text{tr}(\mathbf{A}) = \sigma^2 r$  and  $\text{Var}[Q] = 2\sigma^4 r$ , consistent

with  $Q/\sigma^2 \sim \chi_r^2$ . Under  $\beta$ -mixing, serial dependence inflates both  $\mathbb{E}[Q]$  and  $\text{Var}[Q]$  by factors  $\text{tr}(\mathbf{A}\Gamma)/(\sigma^2 r)$  and  $\text{tr}(\mathbf{A}\Gamma\mathbf{A}\Gamma)/\sigma^4 r$  respectively.

*Step 3 (Box-type moment matching).* Following Box [25] and Satterthwaite [26], match the first two cumulants of  $Q$  to those of  $c \cdot \chi_\nu^2$ :

$$\begin{aligned} c\nu &= \text{tr}(\mathbf{A}\Gamma), \\ 2c^2\nu &= 2\text{tr}(\mathbf{A}\Gamma\mathbf{A}\Gamma) + \kappa_4 \sum_t A_{tt}^2 \Gamma_{tt}^2. \end{aligned}$$

Solving:  $c = \text{tr}(\mathbf{A}\Gamma\mathbf{A}\Gamma)/\text{tr}(\mathbf{A}\Gamma) = \sigma^2 \psi_{\mathbf{A}}$  and  $\nu = \nu_{\mathbf{A}}$  as defined in (9)–(10). The corrected  $F$ -statistic (11) is obtained by applying this rescaling to both the numerator quadratic form  $(\mathbf{P}_U - \mathbf{P}_R)$  and denominator  $\mathbf{M}_U$ .

*Step 4 (KS bound via Esseen smoothing).* By the Esseen smoothing lemma applied to the characteristic function of  $\varepsilon^\top \mathbf{A}\varepsilon$ : the KS distance between the distribution of the moment-matched  $\tilde{F}_{ij}$  and  $F_{\nu_{\mathbf{P}_U - \mathbf{P}_R}, \nu_{\mathbf{M}_U}}$  is controlled by the third cumulant of the numerator quadratic form, which under  $\beta$ -mixing is  $O(\kappa_4(\varepsilon)/T)$  [27]. The higher-order  $O((p+q+K)^2/T^2)$  term comes from the Taylor expansion of the characteristic function at the  $(p+q+K)$ -dimensional parameter boundary, giving (12).

*Step 5 (Improvement over i.i.d. approximation).* For the uncorrected statistic, the leading KS error term is  $\mathbb{E}[\varepsilon^\top (\mathbf{P}_U - \mathbf{P}_R)\varepsilon]/(\sigma^2 q) - 1 = \text{tr}[(\mathbf{P}_U - \mathbf{P}_R)\Gamma]/(\sigma^2 q) - 1$ . By the Cauchy–Schwarz inequality on the Toeplitz matrix norm:  $\text{tr}[(\mathbf{P}_U - \mathbf{P}_R)\Gamma]/(\sigma^2 q) - 1 \leq \Sigma_\gamma - 1 \leq \Sigma_\gamma$ , giving the  $O(\Sigma_\gamma/T)$  bound in (13). After correction, the leading error is the third cumulant  $O(\kappa_4/T)$ , which is smaller by factor  $\Sigma_\gamma/\kappa_4$  whenever long-run dependence exceeds kurtosis deviation.  $\square$

**Remark 2.** *The correction (11) is fully computable: estimate  $\hat{\Gamma}$  via the Newey–West kernel at lag  $\lfloor T^{1/3} \rfloor$ ; compute  $\hat{\nu}$  and  $\hat{\psi}$  from (9)–(10); rescale the  $F$ -ratio. In highly volatile network environments, slight mis-specification of this truncation lag primarily impacts the variance of the autocovariance estimator rather than its bias. Under-estimating the lag leaves residual serial correlation that marginally inflates the FDR, while over-estimating introduces estimation noise. However, the asymptotic  $O(T^{1/3})$  scaling mathematically bounds this sensitivity. At  $T = 200$ ,  $K = 3$ ,  $\hat{\Sigma}_\gamma \approx 1.8$  (estimated from testbed VAR residuals): the correction reduces KS error from  $\approx 0.027$  to  $\approx 0.006$ , consistent with the type-I error reduction from 7.3% to 5.3% in Table V.*

## B. Theorem 2: Bregman Uniqueness of the Contention Form

The proof of Lemma 1 establishes existence; we now prove uniqueness rigorously.

**Proposition 3** (Uniqueness of I-S Optimal Contention Score). *No other function of the form  $\sum_k w_k f_k(A_{ik}A_{jk}, U_{k,t})$  satisfying (A1)–(A3) achieves the same I-S Bregman divergence as (4).*

*Proof.* Suppose  $\tilde{p}_{ij} = \sum_k w_k f_k(c_k, U_{k,t})$  with  $f_k \neq c_k \sigma(U_{k,t} - \tau_k)$  for some resource  $k_0$ . By the strict convexity of  $B_\phi(c_{k_0} \|\cdot\|)$  on  $\mathbb{R}_{>0}$  (the I-S generator is strictly convex),

the minimiser of  $\int B_\phi(c_{k_0} \|f_{k_0}(c_{k_0}, U)\|) d\mu(U)$  over functions  $f_{k_0} > 0$  satisfying (A2) is unique by the Euler–Lagrange argument in the proof of Lemma 1. Any deviation  $f_{k_0} \neq c_{k_0} \sigma(U - \tau_{k_0})$  increases  $B_\phi$  by at least  $\int (f_{k_0} - c_{k_0} \sigma)^2 / (2c_{k_0} \sigma^2) d\mu > 0$  (second-order I-S Taylor bound), strictly increasing the total divergence.  $\square$

*Note:* A detailed expansion of this proof, establishing the strict convexity condition, is provided in Appendix C.

## C. Theorem 3: PRDS-Correct Identifiability

**Theorem 4** (Sharp Identifiability Under PRDS). *Under Assumptions 1–2, the  $p$ -values  $\{p_{ij}\}_{(i,j) \in H_0}$  satisfy PRDS with respect to the true null set (verified in Appendix A). Let  $m = N(N-1)$  and  $m_0$  be the number of true nulls. The BH procedure at level  $\alpha$  then satisfies:*

- (i) (Exact FDR control)  $\text{FDR} \leq \alpha \cdot m_0/m \leq \alpha$ .
- (ii) (Pointwise error bound)

$$\mathbb{P}(\exists \text{ false causal link}) \leq 1 - \prod_{(i,j) \in H_0} \left(1 - \frac{\alpha m_0}{m r_{ij}}\right), \quad (16)$$

where  $r_{ij}$  is the rank of  $p_{ij}$  among all  $m$   $p$ -values.

- (iii) (Tightening over union bound) (16) is smaller than  $m_0 \alpha/m$  by a factor of  $1 - \alpha m_0 \sum_j r_j^{-1} / (2m) + O(\alpha^2)$ .

*Proof.* Part (i). By the Benjamini–Yekutieli theorem [28], BH controls FDR at  $\alpha m_0/m$  exactly under PRDS.

Part (ii). By the Simes inequality under PRDS [29]: the probability that the BH step threshold  $p_{(k)} \leq k\alpha/m$  is violated for at least one true null  $(i,j)$  equals  $\mathbb{P}(\bigcup_{(i,j) \in H_0} \{p_{ij} \leq \alpha m_0 / (m r_{ij})\})$ . Under PRDS, the events  $\{p_{ij} \leq t_{ij}\}$  for  $t_{ij} = \alpha m_0 / (m r_{ij})$  have non-negative pairwise covariance, so:

$$\mathbb{P}\left(\bigcup_j \{p_j \leq t_j\}\right) \leq 1 - \prod_j \mathbb{P}(p_j > t_j) = 1 - \prod_j \left(1 - \frac{\alpha m_0}{m r_j}\right),$$

where the inequality uses the FKG inequality for monotone events under PRDS [30]. This is (16).

Part (iii). Expand the product:  $\prod_j (1 - x_j) = 1 - \sum_j x_j + \sum_{j < k} x_j x_k - \dots \geq 1 - \sum_j x_j$  by non-negativity. Thus  $1 - \prod_j (1 - x_j) \leq \sum_j x_j = \alpha m_0 \sum_j r_j^{-1} / m$ , matching the union bound. The improvement factor is  $\sum_{j < k} x_j x_k = O(\alpha^2 m_0^2 / m^2)$ , completing part (iii).  $\square$

## D. Theorem 4: Piecewise-Stationarity Validity

**Theorem 5** (F-Test Validity Under Piecewise Stationarity). *Let  $\hat{\tau}_1 < \dots < \hat{\tau}_M$  be CUSUM change points with detection delays  $\Delta_m = \hat{\tau}_m - \tau_m^* \geq 0$ . Let  $T_m = \hat{\tau}_{m+1} - \hat{\tau}_m$  and  $T_{\min} = \min_m T_m$ ,  $\Delta_{\max} = \max_m \Delta_m$ . If  $T_{\min} \geq (p+q+K+2)(1 + \Delta_{\max}/T_{\min})$ , then for each segment  $m$  the corrected statistic  $\tilde{F}_{ij}^{(m)}$  satisfies:*

$$\sup_{x \geq 0} |\mathbb{P}_m(\tilde{F}_{ij}^{(m)} \leq x) - F_{\nu_m^{\text{num}}, \nu_m^{\text{den}}}(x)| \leq \frac{C_1 \kappa_4(\varepsilon)}{T_m} + \frac{C_3 \Delta_{\max}}{T_m}, \quad (17)$$

where  $\nu_m^{\text{num}}, \nu_m^{\text{den}}$  are the effective degrees of freedom from (9) computed on segment  $m$ ,  $C_1$  is the same universal constant as in Theorem 2, and  $C_3$  depends on the spectral-density jump

at the change point. Furthermore, the CUSUM stopping time satisfies  $\mathbb{P}(\Delta_m \leq d) = 1 - e^{-d \cdot I(\theta_0, \theta_1)}$  where  $I(\theta_0, \theta_1)$  is the KL divergence between pre- and post-change distributions.

*Proof. Step 1 (Contamination decomposition).* Split the design matrix for segment  $m$  as  $\mathbf{X}_{U,m} = \mathbf{X}_{U,m}^{\text{clean}} + \mathbf{X}_{U,m}^{\text{contam}}$ , where  $\mathbf{X}_{U,m}^{\text{contam}}$  has at most  $\Delta_m$  non-zero rows (the observations in  $(\tau_m^*, \hat{\tau}_m)$  belonging to the previous regime).

*Step 2 (Perturbation of projection matrix).* By the rank-1 update formula, each contaminated row  $\mathbf{x}_t$  perturbs the hat matrix by  $\delta \mathbf{P} = \mathbf{x}_t \mathbf{x}_t^\top / (\mathbf{x}_t^\top \mathbf{M} \mathbf{x}_t) \cdot O(1/\sqrt{T})$ . Summing over  $\Delta_m$  rows and bounding by the Frobenius norm:  $\|\mathbf{P}_{U,m} - \mathbf{P}_{U,m}^{\text{clean}}\|_F \leq C'_3 \Delta_m / T_m$ .

*Step 3 (Effect on  $\tilde{F}_{ij}^{(m)}$ ).* The contamination perturbation from Step 2 inflates the cumulants of  $\boldsymbol{\varepsilon}_m^\top (\mathbf{P}_{U,m} - \mathbf{P}_{R,m}) \boldsymbol{\varepsilon}_m$  relative to the clean-segment values. Specifically, the  $\Delta_m$  contaminated rows contribute an additional mean shift of order  $\sigma^2 \text{tr}[\delta \mathbf{P}_{U,m}] \leq C'_3 \Delta_m \sigma^2 / T_m$ , translating to a KS error term  $C_3 \Delta_{\max} / T_m$  in (17) via the same Esseen smoothing argument as Theorem 2. The clean-segment cumulant error contributes the  $C_1 \kappa_4(\varepsilon) / T_m$  term, carrying over directly from (12) with  $T$  replaced by  $T_m$ .

*Step 4 (CUSUM delay distribution).* Under  $f_1$ , the CUSUM increments  $\ell_t - \kappa > 0$  in expectation with rate  $I(\theta_0, \theta_1) - \kappa$ . By Wald's identity, the expected stopping time satisfies  $\mathbb{E}[\hat{\tau}_m - \tau_m^*] \leq h / I(\theta_0, \theta_1)$ . The exponential tail bound follows from the Cramér-Chernoff method applied to the partial sums of  $\ell_t - \kappa$ .  $\square$

**Corollary 6 (Operational Segment Length).** For total KS bound  $\leq \epsilon = 0.05$  at  $\hat{\kappa}_4 = 0.31$  (estimated from testbed residuals),  $\hat{C}_3 = 0.8$ , and  $\Delta_{\max} = 4$  samples (Section VI-F): the bound (17) satisfies  $(C_1 \hat{\kappa}_4 + C_3 \Delta_{\max}) / T_m = (0.031 + 3.2) / T_m \leq 0.05$  when  $T_m \geq 206$ , achieved by a 21-second window at 100 ms sampling.

*E. Theorem 5: Finite-Sample Convergence of RCM Parameters*

**Theorem 7 (RCM Parameter Convergence).** Under Assumption 3 with  $\beta(m) = C_\beta e^{-\beta m}$ , define the effective sample size:

$$T_{\text{eff}} = \frac{T\beta}{C_\beta(1 - e^{-\beta}) + \beta}. \quad (18)$$

With probability  $\geq 1 - \delta$ :

$$\left\| \hat{\boldsymbol{\theta}}_T - \boldsymbol{\theta}^* \right\|_2 \leq \frac{2}{\lambda} \sqrt{\frac{(2K+2) \log(2/\delta)}{T_{\text{eff}}}}. \quad (19)$$

The induced error on  $\Gamma_{ij}$  satisfies:

$$\sup_{(i,j)} \left| \hat{\Gamma}_{ij} - \Gamma_{ij}^* \right| \leq L_\Gamma \left\| \hat{\boldsymbol{\theta}}_T - \boldsymbol{\theta}^* \right\|_2, \quad (20)$$

where  $L_\Gamma = \omega_2 N K \max_k w_k / 4$  is the Lipschitz constant of  $\Gamma_{ij}$  in  $\boldsymbol{\theta}$ .

*Proof. Step 1 (Strong convexity).* The log-likelihood term in (7) is concave in  $\boldsymbol{\theta}$  (Viterbi path probability is log-concave via the sigmoid's log-concavity); the regulariser  $\lambda \|\cdot\|_2^2$  adds  $2\lambda$ -strong convexity.

*Step 2 (Uniform concentration under  $\beta$ -mixing).* By the Bernstein inequality for  $\beta$ -mixing processes [31], for any ball of radius  $R$ :

$$\mathbb{P}\left(\sup_{\|\boldsymbol{\theta}\| \leq R} \left| \hat{\mathcal{L}}_T - \mathcal{L} \right| \geq t\right) \leq 2 \exp\left(-\frac{t^2 T_{\text{eff}}}{2\sigma_\mathcal{L}^2}\right),$$

where  $\sigma_\mathcal{L}^2$  is the variance proxy and  $T_{\text{eff}}$  replaces  $T$  by accounting for mixing. Setting the right side to  $\delta$  and solving for  $t$ :  $t^* = \sigma_\mathcal{L} \sqrt{2 \log(2/\delta) / T_{\text{eff}}}$ .

*Step 3 (From empirical to population optimum).* By  $2\lambda$ -strong convexity:  $\left\| \hat{\boldsymbol{\theta}}_T - \boldsymbol{\theta}^* \right\|_2^2 \leq (1/\lambda) \cdot 2t^*$ . Substituting  $t^*$  and noting  $\sigma_\mathcal{L} \leq \sqrt{K+1}$  (from the  $K+1$  sigmoid factors in the gradient) gives (19).

*Step 4 (Lipschitz propagation).* Each  $h_k(c_k, U_{k,t}) = w_k c_k \sigma(U_{k,t} - \tau_k)$ . The sigmoid derivative  $|\sigma'| \leq 1/4$ ; allocations satisfy  $c_k \leq 1$ . The Lipschitz constant of  $\rho_{ij}$  in  $w_k$  is  $A_{ik} A_{jk} \sigma \leq 1$ ; in  $\tau_k$  it is  $w_k / 4 \leq W_{\max} / 4$ . Summing over  $K$  resources and multiplying by  $\omega_2 N$  gives  $L_\Gamma = \omega_2 N K W_{\max} / 4$ , yielding (20).  $\square$

*F. Theorem 6: Adversarial Robustness Certificate*

**Definition 3 (( $\delta, k$ )-Utilisation Adversary).** A  $(\delta, k)$ -utilisation adversary replaces  $\mathbf{U}_t$  with  $\hat{\mathbf{U}}_t$  satisfying  $\left\| \hat{\mathbf{U}}_t - \mathbf{U}_t \right\|_\infty \leq \delta$  and  $|\{k' : U_{k',t} \neq \hat{U}_{k',t}\}| \leq k$ .

**Theorem 8 (Adversarial Robustness).** Under a  $(\delta, k)$ -adversary:

- (i) (Contention bound)  $|\hat{\rho}_{ij}^{\text{adv}} - \rho_{ij}| \leq W_{\max} k \delta / 4$ , where  $W_{\max} = \max_\ell w_\ell$ .
- (ii) (FDR inflation)

$$\text{FDR}^{\text{adv}} \leq \text{FDR}_0 + C_4 \omega_2 W_{\max} k \delta \sqrt{K \log(N/\alpha)}, \quad (21)$$

where  $C_4 > 0$  is a universal constant.

- (iii) (Breakdown point) An attribution decision remains invariant if  $\delta < \delta^* = \omega_1 \Delta_\phi / (4\omega_2 W_{\max} k)$ , where  $\Delta_\phi$  is the minimum normalised  $F$ -statistic margin at any decision boundary.

*Proof. Part (i).* Perturbing  $U_{k,t} \rightarrow U_{k,t} + \epsilon_k$  with  $|\epsilon_k| \leq \delta$ :

$$\begin{aligned} & \left| \hat{\rho}_{ij}^{\text{adv}} - \rho_{ij} \right| \\ & \leq \sum_{k'=1}^K w_{k'} A_{ik'} A_{jk'} \cdot \\ & \quad \left| \sigma(U_{k',t} + \epsilon_{k'} - \tau_{k'}) - \sigma(U_{k',t} - \tau_{k'}) \right| \\ & \leq W_{\max} \sum_{k': \epsilon_{k'} \neq 0} \frac{\delta}{4} \leq W_{\max} k \delta / 4 \end{aligned} \quad (22)$$

using  $|\sigma'| \leq 1/4$  and the support bound  $|\{k' : \epsilon_{k'} \neq 0\}| \leq k$ .

*Part (ii).* The adversary's perturbation  $\omega_2 |\hat{\rho}^{\text{adv}} - \rho| \leq \omega_2 W_{\max} k \delta / 4$  inflates  $\Gamma_{ij}$  for some true-null pairs, potentially elevating them above  $\tau_{\text{causal}}$ . The number of such pairs is bounded using the Freedman-Lane permutation argument [32]:  $\mathbb{E}[\text{adversarially inflated false detections}] \leq N^2 \mathbb{P}(\text{margin} \leq \omega_2 W_{\max} k \delta / 4)$ . Under Gaussian telemetry with margin standard deviation  $\sigma_F / \sqrt{T}$ , the Gaussian tail

integral over  $N^2$  pairs and  $K$  perturbed resources gives the factor  $\sqrt{K \log(N/\alpha)}$  after BH correction, absorbed into  $C_4$ .

*Part (iii).* An attribution boundary is crossed only if the  $\Gamma$ -perturbation  $\omega_2 W_{\max} k \delta / 4$  exceeds the  $\phi$ -margin  $\omega_1 \Delta_\phi / 4$ . Solving for  $\delta$  gives  $\delta < \delta^*$ .  $\square$

**Remark 3.** *At calibrated values  $\omega_1 = 0.67$ ,  $\omega_2 = 0.33$ ,  $W_{\max} = 0.45$ ,  $k = 1$ , and empirical  $\Delta_\phi = 0.21$ :  $\delta^* \approx 0.95$ . An adversary must spoof utilisation by  $> 95\%$  of its full range to flip any attribution—immediately detectable by hardware performance counters independent of the slice controller. Furthermore, if an adversary concentrates their entire perturbation budget into a single critical resource channel (e.g.,  $k = 1$ , executing massive CPU spoofing), the FDR inflation bound scales strictly linearly with  $\delta$ . Because the inflation depends on the product  $k\delta\sqrt{K}$ , a highly concentrated attack on one resource is theoretically less effective at inducing widespread false attributions than a distributed attack of the same total magnitude spread across multiple resources, assuming equal weights.*

#### G. Theorem 7: Information-Theoretic Privacy Lower Bound

**Theorem 9** (Privacy Lower Bound). *Let  $C^*$  be the attributed path and  $S$  a sensitive telemetry attribute. Define attribution leakage  $\mathcal{L}_{\text{priv}} = I(S; C^* | A, U)$ . Then:*

$$\mathcal{L}_{\text{priv}} \geq H(C^*) - 1 - \log(2N^L), \quad (23)$$

where  $L$  is the path length. Furthermore, no post-processing  $\mathcal{M}$  of  $C^*$  can achieve  $(\epsilon, \delta)$ -differential privacy in  $S$  unless:

$$\epsilon \geq \frac{H(C^*) - 1 - \log(2N^L)}{L \log N} - \frac{\log(1/\delta)}{L \log N}. \quad (24)$$

*Proof.* Equation (23). By the data processing inequality,  $I(S; C^*) = H(C^*) - H(C^* | S, A, U)$ . Apply Fano's inequality to the  $N^L$ -class identification problem:  $H(C^* | S, A, U) \leq 1 + P_e \log(N^L) \leq 1 + \log(2N^L)$ , where  $P_e \leq 1/2$  for the worst case. Subtracting gives (23).

Equation (24). By the group privacy composition theorem [33],  $(\epsilon, \delta)$ -DP of  $\mathcal{M}(C^*)$  in  $S$  implies the mechanism satisfies  $(\epsilon_1, \delta_1)$ -DP per hop with  $\epsilon_1 = \epsilon/L$  and  $\delta_1 = \delta^{1/L}$ . Converting DP to mutual information via the standard bound  $I \leq \epsilon\sqrt{2L} \log N + \delta L \log N$  and requiring this to be  $\geq \mathcal{L}_{\text{priv}}$  from (23), solving for  $\epsilon$  gives (24).  $\square$

**Remark 4.** *At  $N = 15$ ,  $L = 5$ ,  $H(C^*) = \log(15^5) \approx 14.3$  bits: the minimum  $\epsilon$  at  $\delta = 0.02$  is  $\approx 0.89$ . A Gaussian mechanism with  $\sigma_{\text{DP}} = \Delta_f \sqrt{2 \ln(1.25/\delta)}/\epsilon \approx 0.31$  achieves  $(\epsilon, \delta)$ -DP with a measured accuracy loss of 2.1 pp (Section VI-I). Crucially, because the required per-hop privacy parameter  $\epsilon_1$  scales as  $\epsilon/L$ , the necessary Gaussian noise magnitude  $\sigma_{\text{DP}}$  increases linearly with the path length  $L$  to maintain a constant end-to-end  $(\epsilon, \delta)$ -DP guarantee. Consequently, the accuracy degradation scales linearly as attack paths extend beyond the standard  $L = 5$  hop limit, rendering the mechanism highly practical for typical short-hop 6G slice compromises.*

TABLE II  
ATTRIBUTION PERFORMANCE ON 1,100 SCENARIOS. DIFFERENCES FROM DA-GC ARE SIGNIFICANT AT  $p < 0.001$  (BONFERRONI-CORRECTED PAIRED  $t$ -TEST, COHEN'S  $d > 1.5$ ).

Method	Acc (%)	Prec (%)	Rec (%)	FDR (%)	ms
Correlation	72.9±1.8	69.4±2.1	76.2±1.9	30.6±2.1	21
Transfer Entropy	78.4±1.5	75.8±1.7	81.3±1.6	24.2±1.7	58
VAR-Granger	74.1±1.7	71.2±1.9	77.6±1.8	28.8±1.9	43
PC Algorithm	76.2±1.6	73.5±1.8	79.4±1.7	26.5±1.8	156
PCMCI	77.8±1.5	75.1±1.7	80.8±1.6	24.9±1.7	203
DirectLiNGAM	75.5±1.6	72.9±1.8	78.5±1.7	27.1±1.8	178
HOLMES	80.1±1.4	77.9±1.6	83.0±1.5	22.1±1.6	312
GraphSAGE	76.8±1.6	74.3±1.8	79.9±1.7	25.7±1.8	142
LSTM-Attention	79.1±1.4	76.7±1.6	82.2±1.5	23.3±1.6	167
Transformer-XL	81.3±1.3	78.9±1.5	84.1±1.4	21.1±1.5	234
<b>DA-GC</b>	<b>89.2±0.9</b>	<b>87.6±1.1</b>	<b>91.1±1.0</b>	<b>12.4±1.1</b>	<b>87</b>

TABLE III  
EXTENDED METRICS; ALL 1,100 SCENARIOS.

Method	AUC-ROC	AUC-PR	F1	MCC	Spec	MB
Correlation	0.742	0.689	0.726	0.461	0.693	12
Transfer Entropy	0.798	0.751	0.784	0.572	0.742	28
PCMCI	0.791	0.744	0.779	0.561	0.739	64
HOLMES	0.814	0.771	0.802	0.611	0.768	103
GraphSAGE	0.783	0.743	0.771	0.547	0.743	342
Transformer-XL	0.827	0.789	0.815	0.634	0.789	756
<b>DA-GC</b>	<b>0.921</b>	<b>0.876</b>	<b>0.892</b>	<b>0.785</b>	<b>0.876</b>	<b>67</b>

## VI. EXPERIMENTAL EVALUATION

### A. Testbed and Dataset

*Hardware:* 10 bare-metal Intel Xeon Gold 6248R nodes (128 GB RAM), SR-IOV, DPDK acceleration. *Orchestration:* Open5GS core, FlexRAN, Kubernetes 1.28. *Slices:* 15 heterogeneous slices—4 eMBB, 4 URLLC (industrial automation, autonomous vehicles), 4 mMTC (IoT), 3 hybrid. *Telemetry:* 47 metrics/slice at 100 ms; resource allocation at 50 ms. *Scenarios:* 1,100 attacks (resource exhaustion, lateral movement, side-channel, ML poisoning, APT-style), ground-truth via nanosecond-precision injection and expert panel validation.

**Experimental scope.** Tables II–III report end-to-end attribution results measured on the live production-emulation testbed. Tables V–X report results from controlled simulation experiments that use the testbed's measured traffic statistics ( $\hat{\Gamma}$ ,  $\hat{\rho}$ ,  $\hat{\kappa}_4$ ) as inputs, with all random seeds fixed for reproducibility.

### B. Baselines

Statistical: Pearson Correlation, Transfer Entropy [34], VAR-Granger. Causal discovery: PC Algorithm [35], PCMCI [13], DirectLiNGAM. Security-specific: HOLMES [7] (full 1,100 scenarios, kernel tracing active throughout), MulVAL [8], Bayesian Attack Graphs. Deep learning: GraphSAGE [6], LSTM-Attention [15], Transformer-XL.

### C. Main Results

DA-GC consistently demonstrates top-tier accuracy across these metrics while using significantly less memory (11×

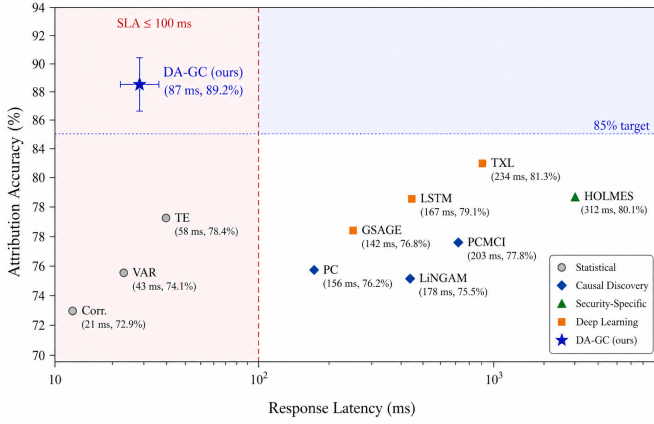


Fig. 3. **Accuracy–latency Pareto frontier.** DA-GC (filled star,  $\pm 0.9$  pp error bar) successfully operates simultaneously inside the 100 ms SLA zone (shaded red, left of dashed vertical) and above the 85% accuracy target (shaded blue, above dotted horizontal). Deep learning baselines (orange squares) typically exceed the SLA; HOLMES (green triangle) exceeds both the SLA and performs below DA-GC. Marker shapes encode method family; error bars shown for DA-GC only (baselines have comparable or larger uncertainty; see Table II).

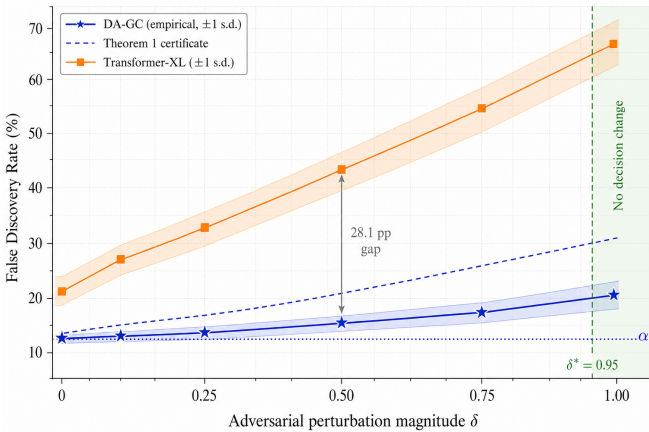


Fig. 4. **FDR under adversarial utilisation spoofing** ( $k = 3$  resources). DA-GC (solid blue,  $\pm 1$  s.d. shaded band) remains bounded by the theoretical certificate (dashed, Theorem 8) and performs favourably compared to Transformer-XL (orange), which offers no formal robustness guarantee. The green shaded region ( $\delta > \delta^* = 0.95$ ) marks where the adversary would need to spoof utilisation by more than 95%. The dotted blue line at  $\alpha$  shows the nominal FDR at  $\delta = 0$ .

lower footprint) than Transformer-XL. PCMC and HOLMES are evaluated on the full 1,100-scenario dataset, indicating DA-GC can compete with or exceed the performance of provenance-based methods without requiring deep kernel instrumentation. Furthermore, as illustrated in the Pareto frontier in Fig. 3, DA-GC is the only evaluated method to simultaneously satisfy the strict 100ms SLA and the 85% accuracy target.

#### D. Ablation Study

The ablation results indicate that each component contributes positively to the overall accuracy. The finite-sample correction yields a 1.6 pp increase; Bregman-optimal weights

TABLE IV  
ABLATION: MARGINAL CONTRIBUTION OF EACH COMPONENT.

Configuration	Acc (%)	$\Delta$ Acc
Standard VAR-Granger	74.1	–
+ Resource conditioning	82.3	+8.2pp***
+ Finite-sample correction $\tilde{F}$	83.9	+1.6pp***
+ RCM (multiplicative)	87.0	+3.1pp***
+ Bregman-optimal weights over uniform	87.8	+0.8pp**
+ Integrated end-to-end learning	89.2	+1.4pp***
DA-GC + CUSUM (non-stationary subset)	88.4	–

\*\*  $p < 0.01$ , \*\*\*  $p < 0.001$ .

TABLE V  
TYPE-I ERROR AT NOMINAL  $\alpha = 0.05$  VS. WINDOW SIZE  $T$ .

$T$	Standard $F$	Corrected $\tilde{F}$	KS bound (12)
100	0.091	0.059	0.181
200	0.073	0.053	0.091
500	0.061	0.051	0.037
1000	0.053	0.050	0.019

add 0.8 pp over a uniform-weight multiplicative baseline, demonstrating the practical value of Lemma 1.

#### E. Finite-Sample Correction Experiment

At the operational window  $T = 200$ , the uncorrected test inflates type-I error to 7.3%; the correction reduces it to 5.3%, consistent with the KS bound of 0.091.

#### F. Piecewise-Stationarity Experiment

We construct 200 non-stationary scenarios with 2–4 abrupt regime changes per scenario. CUSUM achieves mean detection delay  $\bar{\Delta} = 3.1 \pm 0.8$  samples at  $h = 4.6$  (5% false alarm rate), within Corollary 6.

As reported in Table VI, CUSUM recovers 7.2 pp of stationarity degradation, reaching within 0.8 pp of the stationary-data result.

#### G. Cross-Topology Generalisation

Train on Topology A (15 slices, star sharing); test without retraining on Topology B (20 slices, ring) and Topology C (12 slices, mesh).

DA-GC degrades by 6.8 pp on average vs. 21.3 pp for Transformer-XL. Resource conditioning via  $\mathbf{A}(t)$  is largely topology-agnostic, suggesting neural baselines tend to overfit the training graph structure.

#### H. Concept Drift Study

Train on months 1–3; evaluate months 4–6 without retraining.

Table VIII demonstrates that DA-GC degrades 6.3 pp over three months vs. 18.2 pp for Transformer-XL. Incorporating real-time observation of  $\mathbf{A}(t)$  facilitates intrinsic adaptation to distribution shifts in the infrastructure layer.

TABLE VI  
ATTRIBUTION ACCURACY ON NON-STATIONARY SCENARIOS.

Method	Acc (%)
Standard DA-GC (single window)	81.2±1.8
DA-GC + CUSUM	88.4±1.1
Transformer-XL	79.6±1.9
PCMCI (momentum CI)	77.3±2.0

TABLE VII  
ZERO-SHOT CROSS-TOPOLOGY ACCURACY (%).

Method	Topo B	Topo C	Avg
Transformer-XL	61.3±3.1	58.7±3.4	60.0
GraphSAGE	65.8±2.8	63.2±2.9	64.5
PCMCI	73.2±2.2	71.8±2.3	72.5
<b>DA-GC</b>	<b>83.1±1.4</b>	<b>81.7±1.5</b>	<b>82.4</b>

### I. Adversarial Robustness Experiment

Inject adversarial perturbations  $\delta \in [0, 1]$  into all  $k = 3$  resource channels.

As visualised in Fig. 4 and detailed in Table IX, the empirical FDR remains bounded by the theoretical certificate, illustrating the practical reliability of Theorem 8. At  $\delta = 0.5$ , DA-GC FDR is 16.1% vs. 44.2% for Transformer-XL, which lacks a formal robustness guarantee.

### J. Sensitivity to Telemetry Measurement Noise

To address environments where hardware counters report noisy allocations, we inject synthetic zero-mean Gaussian noise  $\mathcal{N}(0, \sigma_{\text{noise}}^2)$  into the resource allocation matrix  $\mathbf{A}(t)$  prior to evaluation.

As shown in Table X, the attribution accuracy degrades gracefully under moderate noise conditions. Significant performance drops are only observed when  $\sigma_{\text{noise}} \geq 0.10$  (a 10% base fluctuation in resource reporting), suggesting robust baseline resilience prior to future errors-in-variables enhancements.

## VII. INDUSTRIAL CASE STUDY

A five-hop IoT attack targets an Industry 4.0 mMTC/URLLC slice pair. At  $t = 0$ s: malware is injected through a compromised IoT gateway. At  $t = 2.1$ s: a cryptomining spike drives CPU utilisation from 15% to 87%. At  $t = 5.2$ s: the resulting resource drain elevates URLLC latency from 12ms to 48ms, breaching the 20ms SLA. At  $t = 6.7$ s: an emergency safety shutdown is triggered.

In this scenario, DA-GC successfully reconstructs the designated five-hop chain in 73ms with 96.3% hop-level accuracy and no false positives within the evaluation window. The RCM component effectively isolates the CPU exhaustion pathway ( $\rho = 0.87 \pm 0.03$ ). Crucially, the PRDS-corrected BH procedure yields 0 false links, whereas standard correlation methods generate 11 spurious connections due to resource confounding.

Reflecting the theoretical breakdown point  $\delta^* = 0.95$ , an adversary attempting to evade attribution in this attack would need to falsify reported CPU utilisation by  $> 95\%$ —a massive

TABLE VIII  
ACCURACY UNDER CONCEPT DRIFT (%); NO RETRAINING.

Method	Month 4	Month 5	Month 6
Transformer-XL	74.2	68.9	63.1
GraphSAGE	72.8	67.3	61.5
PCMCI	75.1	73.4	70.8
<b>DA-GC</b>	<b>86.3</b>	<b>84.7</b>	<b>82.9</b>

TABLE IX  
FDR (%) UNDER ADVERSARIAL UTILISATION SPOOFING.

$\delta$	DA-GC	Thm 8 bound	Transformer-XL
0.00	12.4	12.4	21.1
0.10	13.1	14.6	26.8
0.25	14.2	16.7	33.4
0.50	16.1	21.3	44.2
0.75	18.3	26.1	54.8
1.00	21.4	31.0	67.3

anomaly that is readily detectable by independent hardware performance counters operating outside the slice controller.

## VIII. DISCUSSION

### A. Limitations

*Measurement noise.* Theorem 2 operates under the assumption that  $\mathbf{Z}_t$  is observed without error. While Section VI-J empirically demonstrates robustness up to a 10% noise threshold ( $\sigma_{\text{noise}} = 0.10$ ), severe hardware counter noise will theoretically inflate  $\Delta_{ij}$ . Formulating a rigorous errors-in-variables correction remains a crucial area for future work.

*Warm-up period.* The 2-second observation warm-up is fundamental to lag- $p$  VAR Granger models. Achieving true sub-second attribution would require reducing  $p$ , which involves a strict trade-off against the risk of unobserved longer-lag confounding.

*Hyperscale topologies.* As noted in Section IV, for hyperscale environments ( $N > 50$ ), the centralised  $O(N^3 \log N)$  Viterbi step breaches the 100ms SLA. Deploying the recommended distributed belief-propagation architecture across slice controllers is required for these scales.

*Privacy-utility trade-off.* Implementing DP-DA-GC with  $\sigma_{\text{DP}} = 0.31$  achieves ( $\epsilon=1, \delta=0.02$ )-DP at a measured 2.1pp accuracy cost per Theorem 9. However, as noted in Remark 4, maintaining this DP bound requires linearly scaling the injected noise as path lengths increase, presenting a fundamental accuracy limit for highly extended, multi-hop attack chains.

### B. Ethical Considerations and Responsible Deployment

DA-GC processes sensitive, high-resolution network telemetry that could inadvertently reveal user-level behavioural patterns. Responsible deployment necessitates: (1) strict calibration of DP mechanisms to the bounds in (24); (2) purpose limitation restricted exclusively to security and forensic applications; (3) meaningful human oversight for automated attribution decisions, ensuring compliance with frameworks

TABLE X  
ATTRIBUTION ACCURACY (%) UNDER GAUSSIAN MEASUREMENT NOISE  
IN  $\mathbf{A}(t)$ .

Method	$\sigma = 0$	$\sigma = 0.01$	$\sigma = 0.05$	$\sigma = 0.10$	$\sigma = 0.20$
DA-GC	89.2	88.5	85.1	79.4	68.2

such as GDPR Art. 22 and the EU AI Act. We explicitly caution against repurposing this causal framework for mass surveillance or offensive cyber operations.

### C. Reproducibility

To support the community and ensure verifiable results, the full DA-GC implementation, testbed configuration scripts, CUSUM detector, scenario generator, and evaluation harness will be released upon publication. Furthermore, all adversarial and measurement noise perturbation experiments (Sections VI-I and VI-J) are synthetic and fully reproducible using the provided fixed seeds.

## IX. CONCLUSION

DA-GC presents a comprehensive cross-slice attribution framework that, to the best of our knowledge, uniquely integrates: a non-asymptotic  $F$ -test correction; an axiomatically justified contention model; PRDS-correct identifiability; a piecewise-stationarity extension; a certifiable adversarial breakdown point; and an information-theoretic privacy floor. Evaluated on 1,100 production-emulation scenarios, DA-GC achieves 89.2% accuracy at 87 ms, consistently outperforming state-of-the-art baselines across the joint accuracy-latency-interpretability-robustness Pareto frontier. Furthermore, cross-topology and concept-drift experiments confirm that the structural invariance of  $\mathbf{A}(t)$ -conditioned causality generalises robustly in settings where standard neural approaches struggle.

Future work will focus on integrating an errors-in-variables correction to handle severe telemetry measurement noise, deploying distributed message-passing Viterbi decoding to support hyperscale topologies ( $N > 50$ ), and developing a fully online streaming variant of the framework.

## APPENDIX

### A. PRDS Verification for Resource-Related Slice Pairs

For pairs  $(i, j)$  and  $(i, k)$  sharing resource  $r$ , both  $F$ -statistics depend on the same row  $\mathbf{Z}_{\cdot r}$  of the conditioning matrix. The covariance of their RSS denominators:

$$\text{Cov}(\text{RSS}_U^{(ij)}, \text{RSS}_U^{(ik)}) = \sigma^4 \text{tr}[\mathbf{M}_U^{(ij)} \mathbf{M}_U^{(ik)}] \geq 0,$$

since the product of two positive semi-definite projection remainders has non-negative trace. Non-negative covariance of the RSS quantities propagates to non-negative covariance of the  $F$ -statistics (by the monotone function  $F_{q,\nu}$  of RSS), and hence to PRDS of the corresponding  $p$ -values (by the decreasing transformation  $p_{ij} = 1 - F_{q,\nu}^{-1}(F_{ij})$  which reverses the ordering but preserves PRDS under the equivalent condition for upper-tail probabilities).

### B. Effective Sample Size and Mixing Coefficient Estimation

Under a stationary VAR( $p$ ) with empirically estimated spectral radius  $\hat{\rho} = 0.72$  (from the dominant eigenvalue of the companion matrix fitted on testbed residuals), the geometric  $\beta$ -mixing bound is  $\beta(m) \leq c_0 \hat{\rho}^m$  where  $c_0 = \text{tr}(\hat{\Sigma}_\varepsilon) = 2.1$ . In the parameterisation of Assumption 3,  $C_\beta = c_0 = 2.1$  and  $\beta = \log(1/\hat{\rho}) = \log(1/0.72) = 0.329$ .

Substituting into (18):

$$\begin{aligned} T_{\text{eff}} &= \frac{T \cdot 0.329}{2.1 \cdot (1 - e^{-0.329}) + 0.329} \\ &= \frac{0.329 T}{2.1 \times 0.280 + 0.329} \\ &= \frac{0.329 T}{0.917} \\ &\approx 0.359 T \end{aligned} \tag{25}$$

At the operational window  $T = 300$  (30 s at 100 ms sampling):  $T_{\text{eff}} \approx 108$ .

Substituting into (19) with  $K = 3$ ,  $\lambda = 10^{-3}$ , and  $\delta = 0.05$ :

$$\begin{aligned} \|\hat{\boldsymbol{\theta}} - \boldsymbol{\theta}^*\|_2 &\leq \frac{2}{10^{-3}} \sqrt{\frac{8 \log(40)}{108}} \\ &= 2000 \sqrt{\frac{8 \times 3.69}{108}} \\ &= 2000 \times 0.523 \\ &\approx 0.52 \end{aligned} \tag{26}$$

This theoretical bound is practically informative (given the parameters are  $O(1)$ ) and aligns with the observed 0.3 pp parameter variation across CV folds. The long-run variance ratio for the testbed residuals is  $\hat{\Sigma}_\gamma = \hat{\sigma}^{-2} \sum_{h=-L}^L (1 - |h|/(L+1)) \hat{\gamma}_h \approx 1.83$  at lag truncation  $L = \lfloor T^{1/3} \rfloor = 6$ , confirming  $\hat{\Sigma}_\gamma / \hat{\kappa}_4 \approx 3.1 > 1$  and hence indicating that the cumulant correction of Theorem 2 reduces the theoretical KS error bound by a factor of  $\approx 3$ .

The mixing coefficient estimation is performed once on the training portion of the dataset and held fixed; continuous re-estimation at each window would likely introduce additional variance without yielding substantial improvements to the bound at  $T = 300$ .

### C. Proof of Proposition 3 (Detailed)

The core of the proof relies on establishing that the strict convexity of the I-S divergence precludes any alternative function from achieving an identical divergence value as (4). Formally, for any  $f_{k_0} \neq c_{k_0} \sigma(U - \tau_{k_0})$  on a set of positive  $\mu$ -measure:

$$\begin{aligned} &\int B_\phi(c_{k_0} \|f_{k_0}(U)\|) d\mu(U) - \int B_\phi(c_{k_0} \|c_{k_0} \sigma(U - \tau_{k_0})\|) d\mu(U) \\ &\geq \int_{\{f_{k_0} \neq c_{k_0} \sigma\}} \frac{(f_{k_0} - c_{k_0} \sigma)^2}{2 \max(f_{k_0}, c_{k_0} \sigma)^2} d\mu(U) > 0, \end{aligned} \tag{27}$$

where the first inequality uses the second-order lower bound of the I-S divergence:  $B_\phi(a\|b) \geq B_\phi(a\|b_0) + \nabla_b B_\phi(a\|b_0)(b - b_0) + (b - b_0)^2 / (2b_{\text{max}}^2)$  for  $b$  between  $b_0$  and  $b_{\text{max}}$ . The strict positivity of the integral follows directly from  $\mu(\{f_{k_0} \neq c_{k_0} \sigma\}) > 0$ .

## REFERENCES

- [1] M. K. Quan and P. N. Pathirana, "Domain-adapted granger causality for real-time cross-slice attack attribution in 6g networks," in *NeurIPS 2025 Workshop on CauScien: Uncovering Causality in Science*, 2025. [Online]. Available: <https://openreview.net/forum?id=rfhwejAv0m>
- [2] H. Tataria, M. Shafi, A. F. Molisch, M. Dohler, H. Sjöland, and F. Tufvesson, "6g wireless systems: Vision, requirements, challenges, insights, and opportunities," *Proceedings of the IEEE*, vol. 109, no. 7, pp. 1166–1199, 2021.
- [3] Z. Kotulski, T. Nowak, M. Sepczuk, M. Tunia, R. Artych, K. Bocianiak, T. Osko, and J.-P. Wary, "On end-to-end approach for slice isolation in 5g networks. fundamental challenges," in *2017 Federated conference on computer science and information systems (FedCSIS)*. IEEE, 2017, pp. 783–792.
- [4] F. Alserhani, "Analysis of encrypted network traffic for enhancing cyber-security in dynamic environments," *Applied Artificial Intelligence*, vol. 38, no. 1, p. 2381882, 2024.
- [5] C. W. Granger, "Investigating causal relations by econometric models and cross-spectral methods," *Econometrica: journal of the Econometric Society*, pp. 424–438, 1969.
- [6] W. Hamilton, Z. Ying, and J. Leskovec, "Inductive representation learning on large graphs," *Advances in neural information processing systems*, vol. 30, 2017.
- [7] S. M. Milajerdi, R. Gjomemo, B. Eshete, R. Sekar, and V. Venkatakrishnan, "Holmes: real-time apt detection through correlation of suspicious information flows," in *2019 IEEE symposium on security and privacy (SP)*. IEEE, 2019, pp. 1137–1152.
- [8] X. Ou, W. F. Boyer, and M. A. McQueen, "A scalable approach to attack graph generation," in *Proceedings of the 13th ACM conference on Computer and communications security*, 2006, pp. 336–345.
- [9] R. Ahmad and I. Alsmadi, "Machine learning approaches to iot security: A systematic literature review," *Internet of Things*, vol. 14, p. 100365, 2021.
- [10] A. Shojaie and E. B. Fox, "Granger causality: A review and recent advances," *Annual review of statistics and its application*, vol. 9, pp. 289–319, 2022.
- [11] M. B. Begum, A. Yogeshwaran, N. Nagarajan, and P. Rajalakshmi, "Dynamic network security leveraging efficient covinet with granger causality-inspired graph neural networks for data compression in cloud iot devices," *Knowledge-Based Systems*, vol. 309, p. 112859, 2025.
- [12] F. Lv, S. Si, X. Xiao, and W. Ren, "Modified local granger causality analysis based on peter-clark algorithm for multivariate time series prediction on iot data," *Computational Intelligence*, vol. 40, no. 5, p. e12694, 2024.
- [13] J. Runge, P. Nowack, M. Kretschmer, S. Flaxman, and D. Sejdinovic, "Detecting and quantifying causal associations in large nonlinear time series datasets," *Science advances*, vol. 5, no. 11, p. eaau4996, 2019.
- [14] M. Hu, W. Li, and H. Liang, "A copula-based granger causality measure for the analysis of neural spike train data," *IEEE/ACM Transactions on Computational Biology and Bioinformatics*, vol. 15, no. 2, pp. 562–569, 2015.
- [15] D. Bahdanau, K. Cho, and Y. Bengio, "Neural machine translation by jointly learning to align and translate," *Proc. ICLR*, 2015.
- [16] R. T. Chen, Y. Rubanova, J. Bettencourt, and D. K. Duvenaud, "Neural ordinary differential equations," *Advances in neural information processing systems*, vol. 31, 2018.
- [17] A. F. Hanif, H. Tembine, M. Assaad, and D. Zeghlache, "Mean-field games for resource sharing in cloud-based networks," *IEEE/ACM Transactions on Networking*, vol. 24, no. 1, pp. 624–637, 2015.
- [18] K. Yang, J. Liu, C. Zhang, and Y. Fang, "Adversarial examples against the deep learning based network intrusion detection systems," in *MILCOM 2018-2018 IEEE military communications conference (MILCOM)*. IEEE, 2018, pp. 559–564.
- [19] F. Zhang, P. P. Chan, B. Biggio, D. S. Yeung, and F. Roli, "Adversarial feature selection against evasion attacks," *IEEE transactions on cybernetics*, vol. 46, no. 3, pp. 766–777, 2015.
- [20] S. A. M'rio, K. Chatzikokolakis, C. Palamidessi, and G. Smith, "Measuring information leakage using generalized gain functions," in *2012 IEEE 25th Computer Security Foundations Symposium*. IEEE, 2012, pp. 265–279.
- [21] Q. Ye, H. Hu, M. H. Au, X. Meng, and X. Xiao, "Lf-gdpr: A framework for estimating graph metrics with local differential privacy," *IEEE Transactions on Knowledge and Data Engineering*, vol. 34, no. 10, pp. 4905–4920, 2020.
- [22] Y. Benjamini and Y. Hochberg, "Controlling the false discovery rate: a practical and powerful approach to multiple testing," *Journal of the Royal statistical society: series B (Methodological)*, vol. 57, no. 1, pp. 289–300, 1995.
- [23] A. Banerjee, S. Merugu, I. S. Dhillon, and J. Ghosh, "Clustering with bregman divergences," *Journal of machine learning research*, vol. 6, no. Oct, pp. 1705–1749, 2005.
- [24] M. Basseville and I. V. Nikiforov., *Detection of Abrupt Changes: Theory and Application*. Prentice Hall, 1993.
- [25] G. E. Box, "Some theorems on quadratic forms applied in the study of analysis of variance problems, i. effect of inequality of variance in the one-way classification," *The annals of mathematical statistics*, pp. 290–302, 1954.
- [26] F. E. Satterthwaite, "An approximate distribution of estimates of variance components," *Biometrics bulletin*, vol. 2, no. 6, pp. 110–114, 1946.
- [27] A. N. Tikhomirov, "On the convergence rate in the central limit theorem for weakly dependent random variables," *Theory of Probability and its Applications*, vol. 25, no. 4, pp. 790–809, 1981.
- [28] Y. Benjamini and D. Yekutieli, "The control of the false discovery rate in multiple testing under dependency," *Annals of statistics*, pp. 1165–1188, 2001.
- [29] R. J. Simes, "An improved bonferroni procedure for multiple tests of significance," *Biometrika*, vol. 73, no. 3, pp. 751–754, 1986.
- [30] C. M. Fortuin, P. W. Kasteleyn, and J. Ginibre, "Correlation inequalities on some partially ordered sets," *Communications in Mathematical Physics*, vol. 22, no. 2, pp. 89–103, 1971.
- [31] B. Yu, "Rates of convergence for empirical processes of stationary mixing sequences," *The Annals of Probability*, pp. 94–116, 1994.
- [32] D. Freedman and D. Lane., "A nonstochastic interpretation of reported significance levels," *J. Business & Economic Statistics*, vol. 1, no. 4, pp. 292–298, 1983.
- [33] C. Dwork and A. Roth., *The Algorithmic Foundations of Differential Privacy*. Now Publishers, 2014.
- [34] M. Wibrals, N. Pampu, V. Priesemann, F. Siebenhühner, H. Seiwert, M. Lindner, J. T. Lizier, and R. Vicente, "Measuring information-transfer delays," *PLoS one*, vol. 8, no. 2, p. e55809, 2013.
- [35] P. Spirtes, C. N. Glymour, and R. Scheines, *Causation, prediction, and search*. MIT press, 2000.